ACS APPLIED MATERIALS & INTERFACES

Research Article

www.acsami.org

Metal Mesh Device Sensor Immobilized with a Trimethoxysilane-Containing Glycopolymer for Label-Free Detection of Proteins and Bacteria

Hirokazu Seto,[†] Seiji Kamba,[‡] Takashi Kondo,[‡] Makoto Hasegawa,[§] Shigeki Nashima,[⊥] Yoshinobu Ehara,[⊥] Yuichi Ogawa,[#] Yu Hoshino,[†] and Yoshiko Miura*[,†]

[†]Graduate School of Engineering, Kyushu University, 744 Motooka, Nishi-ku, Fukuoka, 819-0395, Japan

[‡]Murata Manufacturing Company, 1-10-1 Higashikotari, Nagaokakyo, Kyoto 617-8555, Japan

[§]Graduate School of Bioscience, Nagahama Institute of Bio-Science and Technology, 1266 Tamura, Nagahama, Shiga 526-0829, Japan

[⊥]Graduate School of Engineering, Osaka City University, 3-3-138 Sugimoto, Sumiyoshi-ku, Osaka, 558-8585, Japan

[#]Graduate School of Agriculture, Kyoto University, Kitashirakawaoiwake-cho, Sakyo-ku, Kyoto, 606-8502, Japan

Supporting Information

ABSTRACT: Biosensors for the detection of proteins and bacteria have been developed using glycopolymer-immobilized metal mesh devices. The trimethoxysilane-containing glycopolymer was immobilized onto a metal mesh device using the silane coupling reaction. The surface shape and transmittance properties of the original metal mesh device were maintained following the immobilization of the glycopolymer. The mannose-binding protein (concanavalin A) could be detected at concentrations in the range of 10^{-9} to 10^{-6} mol L^{-1} using the glycopolymer-immobilized metal mesh device sensor, whereas another protein (bovine serum albumin) was not detected. A detection limit of 1 ng mm^{-2} was achieved for the amount of adsorbed concanavalin A. The glycopolymer-immobilized metal mesh device sensor could also detect bacteria as well as protein. The mannose-binding strain of *Escherichia coli* was specifically detected by the glycopolymer-immobilized metal mesh device sensor. The glycopolymer-immobilized metal mesh device could therefore be used as a label-free biosensor showing high levels of selectivity and sensitivity toward proteins and bacteria.

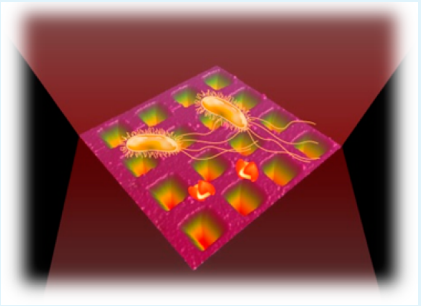

KEYWORDS: *metal mesh device, glycopolymer, label-free biosensor, protein, bacteria*

1. INTRODUCTION

Metal mesh devices (MMDs) have attracted considerable attention in the terms of application as label-free biosensors.[1−6] The surfaces of MMDs are generally composed of well-regulated square holes and indicate the anomalous transmission characteristics. MMDs with grid intervals in the range of tens to hundreds of micrometers can transmit a specific terahertz (THz) wave, and dipped structures can be observed in their IR spectra. The dipped frequency is controlled by the size properties of the MMD, especially their grid interval.[7] The sensing mechanisms of MMDs have been attributed to the localization of an electromagnetic field around their surfaces. The attachment of an analyte to the MMD surface lead to a shift of transmittance spectrum. The thickness of the localized electromagnetic field depends on the dipped frequency of the MMD. For example, 1 THz- and 10 THz-operated MMDs have the $1/e$ decay distances ($L_{1/e}$) of dozens and several micrometers, respectively.[8] The $L_{1/e}$ of the 100 THz-operated MMD corresponds to hundreds of nanometers. When MMD periodic size and light source frequency are chosen so as to fit into the target size, the MMD sensors can be aimed at biomolecules with a wide range of different sizes (from nanosized proteins to microsized cells) based on an identical principle. This is a special characteristic and the biggest advantage as the biosensor. The MMD sensor has a low detection limit (>500 pg mm^{-2}), which is not so different from quartz crystal microbalance (QCM) and surface plasmon resonance (SPR). The MMDs can be manufactured from a wide variety of different metals, because the metal species used in these devices has a low impact on their transmittance properties. Furthermore, given that the FT-IR measurement used in MMD sensing can be conducted in a high-throughput manner and has broad utility, MMDs represent a rapid and facile analytical technique compared with QCM and SPR.

In previous studies of MMD sensors, protein analytes have been trapped on the surfaces of the MMDs through a process of effectively infiltrating the membranes placed on the surfaces of the MMDs[1,3] or physical coating.[2,4,5] It is generally accepted, however, that these methods only provide low levels of selectivity for the detection of biomolecule analytes. Therefore,

Received: May 20, 2014
Accepted: July 11, 2014
Published: July 11, 2014

dx.doi.org/10.1021/am503003v | ACS Appl. Mater. Interfaces 2014, 6, 13234−13241

modifications to the MMD surface are required to achieve higher levels of selectivity. Because the thickness of the electromagnetic field is inversely proportional to the operational frequency, the MMDs are operated at as high frequency as possible so that they are suitable for the detection of small biomolecules. We recently developed a biotin-containing MMD sensor, where the MMD possessed a grid interval of several micrometers and was operated in the middle-infrared frequency range.[6] The binding property of the biotin−streptavidin determined using the MMD sensor was consistent with that determined using the QCM. The MMD measurement was more rapid than the QCM measurement. MMD sensors using bioaffinity can achieve high levels of selective detection for biomolecules.

Saccharides are responsible for molecular recognitions in a wide range of biological phenomena, such as protein binding, cell adhesion, and pathogen infection.[9] The molecular recognition abilities of monovalent saccharides are weak, and saccharides instead have a tendency to prevent the nonspecific adsorption of biomolecules. The interactions of saccharides can be improved by conjugation, which is known as the glyco-cluster effect.[10−12] In fact, saccharides on cell surfaces exist as glycoconjugates, which form the raft- and caveolae-structural systems. Glycopolymers are synthetic polymers, which mimic the functions of saccharides. They also possess large valencies of saccharide, which can effectively lead to the development of the glyco-cluster effect.[13] Various glycosurfaces including the glycopolymer-immobilized surfaces have been widely used as the recognition elements for biosensor and bioanalysis.[14−27]

We have also investigated glycopolymer interfaces possessing biomolecular recognition properties[28] and reported the use of glycopolymer-grafted surfaces as biodevices in biosensing,[29−31] bioseparation,[32,33] and microarray[34] applications. The silane coupling reagent-containing glycopolymer has contributed to the simple preparation of biomaterial.[34] The glycopolymer had mannoside (Man) and trimethoxysilane (TMS) on its side chain and was named as poly(Man-*r*-TMS). Trimethoxysilyl groups can form covalent bonds to hydroxyl groups on surfaces of the variety of different matrices, and the silane coupling reaction is useful for the fabrication of biomaterials for use in biosensing, bioseparation, bioreactor, and micropatterning applications.[34−42] A porous membrane immobilized with poly(Man-*r*-TMS) was prepared using the silane coupling reaction and used to achieve the selective separation of a protein.

In this study, a glycopolymer-immobilized MMD was prepared, and its application as a biosensor for the detection of proteins and bacteria was evaluated in the middle-infrared frequency range. Poly(Man-*r*-TMS) was immobilized on the MMD using the silane coupling reaction. The Man and TMS moieties in the poly(Man-*r*-TMS) were found to play critical roles as the biomolecular-recognition and surface-binding sites, respectively. The selective detection of lectin was investigated using the poly(Man-*r*-TMS)-immobilized MMD sensor. The detectability of *Escherichia coli* (*E. coli*) ORN178 using the poly(Man-*r*-TMS)-immobilized MMD was compared with the mutant *E. coli* ORN208, which does not contains a mannose receptor.

2. EXPERIMENTAL SECTION

2.1. Materials. D-Mannose (Towa Chemical Industry Co. Ltd., Tokyo, Japan), 3-(trimethoxysilyl) propyl methacrylate (TMSMA, Sigma Co., St. Louis, MO, USA), and 2,2′-azobis isobutyronitrile (AIBN, Wako Pure Chemical Industries Ltd., Osaka, Japan) were used for the polymerization process. Albumin from bovine serum (BSA, Sigma Co.) and concanavalin A (Con A, J-Oil Mills Inc., Tokyo, Japan) were used as the protein analytes. Nickel meshes (effective surface area: 67 mm^2) were manufactured by the electroforming method and were used as the MMD, which was operated in the middle-infrared frequency range (Figure S1, Supporting Information). The MMD had an opening length of 1.8 μm, a grid interval of 2.6 μm, and a thickness of ca.1 μm.[6] After UV/O_3 treatment, the MMDs were immersed in an ammonia-hydrogen peroxide mixture (APM) at 60 °C for 20 min, to allow for the formation of an oxidized layer. Nickel-deposited glass slides (nickel thickness: ca. 600 nm) were used for measurement of contact angle and ellipsometry. The transmittance spectra, electromagnetic field distributions, and frequency shift behaviors of the MMD were simulated using the transition line modeling (TLM) and the finite difference time domain (FDTD) methods (see the Supporting Information).

2.2. Immobilization of Poly(Man-*r*-TMS) onto the MMD Surface. Poly(AcMan-*r*-TMS) was obtained using a previously described polymerization method.[32] The nickel meshes were immersed in a poly(AcMan-*r*-TMS) solution (DMF, 5 g L^{-1}, 0.5 mL) at 60 °C for 20 h. To form covalent bonds, the nickel meshes were then heated at 110 °C for 30 min. The immobilized poly(AcMan-*r*-TMS) was deacetylated by immersion in NaOMe solution (MeOH, pH: ca. 10, 1.0 mL) for 30 min. The material was washed with MeOH and dried, to give the poly(Man-*r*-TMS)-immobilized MMD. The successful immobilization of poly(Man-*r*-TMS) on the MMD was confirmed by X-ray photoelectron spectroscopy (XPS, Quantum2000, Physical Electronics, Inc., Chanhassen, MN, USA). The irradiating spot of the X-ray was the frame of the MMD. The XPS spectra were calibrated using the peak corresponding to C−C at 284.6 eV and were peak-divided using the Peak Fit software (v4.12, Systat Software Inc., San Jose, CA, USA). The amount of immobilized poly(Man-*r*-TMS) was estimated from the change in the weight of the MMD. The surface morphology of the poly(Man-*r*-TMS)-immobilized MMD was observed by atomic force microscopy (AFM, Dimension Icon AFM, Bruker AXS, Karlsruhe, Germany) using tapping mode with an antimony-doped Si probe (spring constant: 20−80 N m^{-1}, NCHV-10, Bruker AXS K.K., Yokohama, Japan) under dry conditions. The root mean-square roughness (R_q) and ten-point average roughness (R_z) values were analyzed using NanoScope Analysis software (Bruker AXS). The transmittance IR spectra of the MMDs were determined using an IR spectrometer (Spectrum 100 FTIR Spectrometer, PerkinElmer Inc., Waltham, MA, USA) under dry conditions. The wavenumber resolution, accumulation number, and determining diameter values were 2 cm^{-1}, 8 measurements, and 6 mm ϕ, respectively. The thickness of the polymer on the Ni surface was determined by an ellipsometric measurement (NL-MIE, Nippon Laser & Electronics Lab., Nagoya, Japan) under dry conditions. The reflective index of poly(Man-*r*-TMS) was replaced by that of poly(*N*-phenylacrylamide).

2.3. Adsorption of Protein onto the Poly(Man-*r*-TMS)-Immobilized MMD. The protein analytes, Con A and BSA, were detected using the poly(Man-*r*-TMS)-immobilized MMD. The poly(Man-*r*-TMS)-immobilized MMDs were added to phosphate-buffered saline solutions (pH 7.4) of protein at a variety of different concentrations and then incubated for 3 h. The MMDs were subsequently washed with a sufficient quantity of water and dried. The transmittance IR spectra of the MMDs were determined under dry conditions before and after the protein adsorption process. The frequency shift ($-\Delta f$) and the transmittance changes ($-\Delta T$) were calculated from the differences in the dipped structures before and after the protein adsorption process and were corrected according to those observed for the MMD incubated in the buffer.

The amounts of Con A adsorbed (q) were determined following the elution from the MMDs. Two sheets of the MMDs, which had been subjected to the adsorption process with Con A, were immersed in the eluent at 98 °C for 5 min. The resulting solutions were spotted onto the poly(acrylamide) gel, which was then fractionated by electrophoresis for 1 h. The Con A on the gel was visualized using a staining

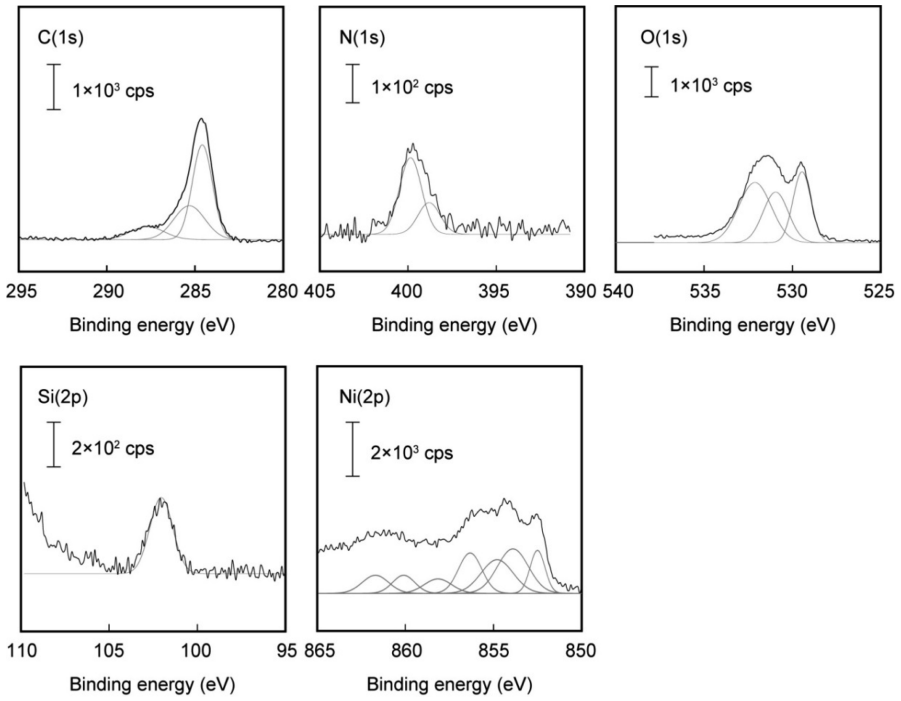

Figure 1. Peak-divided XPS spectra of the poly(Man-*r*-TMS)-immobilized MMD.

reagent, and the gel was then scanned using a fluorescent scanner. The values of q were estimated from the total gray values of the electrophoretic bands, which were obtained using the ImageJ software (National Institutes of Health, Bethesda, MD, USA).

2.4. Detection of Protein Using Poly(Man-*r*-TMS)-Immobilized QCM and SPR Sensors. The surface of the Au oscillator in the QCM cell (Initium Inc., Tokyo, Japan) was cleaned with a drop of piranha solution (i.e., 3:1 v/v mixture of sulfuric acid and hydrogen peroxide). (*CAUTION*: "Piranha" solution reacts violently with organic materials; it must be handled with extreme care.) The QCM cells were suffused with a solution of (3-mercaptopropyl)-trimethoxysilane (Tokyo Chemical Industry Co. Ltd., Tokyo, Japan) in ethanol (10 g L^{-1}, 0.5 mL) and then were incubated at 60 °C for 3 h. The resulting cells were treated with 100 mmol L^{-1} HCl. A solution of poly(AcMan-*r*-TMS) in DMF (5 g L^{-1}, 10 μL) was added dropwise to the surface of oscillator, and the cells were heated at 60 °C for 17 h and at 110 °C for 30 min. The poly(AcMan-*r*-TMS) material was deacetylated by the addition of a solution of NaOMe in MeOH (pH: ~10, 0.5 mL), followed by 30 min of stirring at ambient temperature. The poly(Man-*r*-TMS)-immobilized surface for SPR measurements was prepared according to the method described above using the SIA kit Au chip (GE Healthcare UK Ltd., Little Chalfont, UK).

The adsorption behaviors of different proteins on the poly(Man-*r*-TMS)-immobilized surface were evaluated using QCM (AFFINIX Q4, Initium Inc.) and SPR (Biacore X100 system, GE Healthcare UK Ltd.) measurements at 25 °C. For the QCM measurements, the cell was suffused with phosphate-buffered saline solution (pH: 7.4) and subsequently held at room temperature until the frequency reached equilibrium. The concentrations of Con A and BSA in the QCM cell were enhanced by the sequential injection of protein solutions, and frequency changes ($-\Delta F$) were recorded. For the SPR measurements, HBS-EP$^+$ buffer (10 mmol L^{-1} HEPES, pH 7.4, 3 mmol L^{-1} ethylenediamine tetraacetic acid, 150 mmol L^{-1} NaCl, 0.05% Tween 20) was used as the running buffer. A variety of different concentrations of Con A and BSA was injected at a continuous flow rate of 30 μL min^{-1}, and the SPR responses were recorded. The surface of sensor chip was regenerated by the injection of a 10 mmol L^{-1} HCl.

2.5. Adhesion of Bacteria onto the Poly(Man-*r*-TMS)-Immobilized MMD. Two strains of *E. coli* (ORN178 and ORN208) were used as a bacterial analyte and the corresponding negative control, respectively. The ORN178 strain possesses the wild-type *FimH* domain, which behaves as a mannose receptor on the pili.[43] In contrast, the ORN208 strain is a mutant strain, which does not contain the *FimH* domain, and it cannot bind to mannose. The ORN178 and ORN208 strains were grown in LB media (20 mL) at 37 °C, until the optical densities of the cultures at 600 nm (OD_{600}) reached 0.8. The culture media were subsequently removed by centrifugation at 3500 rpm for 7 min, and the *E. coli* were dispersed in phosphate-buffered solution (pH: 7.4). This procedure was repeated three times to give the corresponding *E. coli* suspensions.

The ORN178 and ORN208 strains were detected using the poly(Man-*r*-TMS)-immobilized MMD. The poly(Man-*r*-TMS)-immobilized MMDs were added to the *E. coli* suspensions at a variety of different concentrations and incubated for 3 h. The MMDs were then washed with a sufficient quantity of water and dried. The transmittance IR spectra of the MMDs were determined under dry conditions before and after the *E. coli* adhesion process, to obtain $-\Delta f$ and $-\Delta T$.

3. RESULTS AND DISCUSSION

3.1. Surficial Characteristics of the Poly(Man-*r*-TMS)-Immobilized MMD. The presence of poly(Man-*r*-TMS) on the MMD was confirmed by XPS. The XPS spectra of the poly(Man-*r*-TMS)-immobilized MMD are shown in Figure 1. In the C(1s) spectrum, the peaks were divided into C−C (284.6 eV), C−N (285.3 eV), and C═O (287.7 eV) bonds. In the N(1s) spectrum, the peak corresponding to N−C bonds of the amide groups was observed around 400 eV. Three peaks were observed in the O(1s) spectrum, which corresponded to the O−Si (531.9 eV), O═C (531.0 eV), and metal oxide (529.7 eV) bonds. The appearance of a peak corresponding to the Si−C bond, which was not observed in the spectrum of the unmodified MMD (Figure S2, Supporting Information), indicated that the trimethoxysilane-containing glycopolymer had been successfully immobilized on the surface. The characterization of the Ni(2p) spectrum has been reported previously by Grosvenor et al.,[44] where the peak at 854.7 eV has been assigned to NiO. The APM treatment led to the formation of an oxidized layer on the Ni surface. Immobiliza-

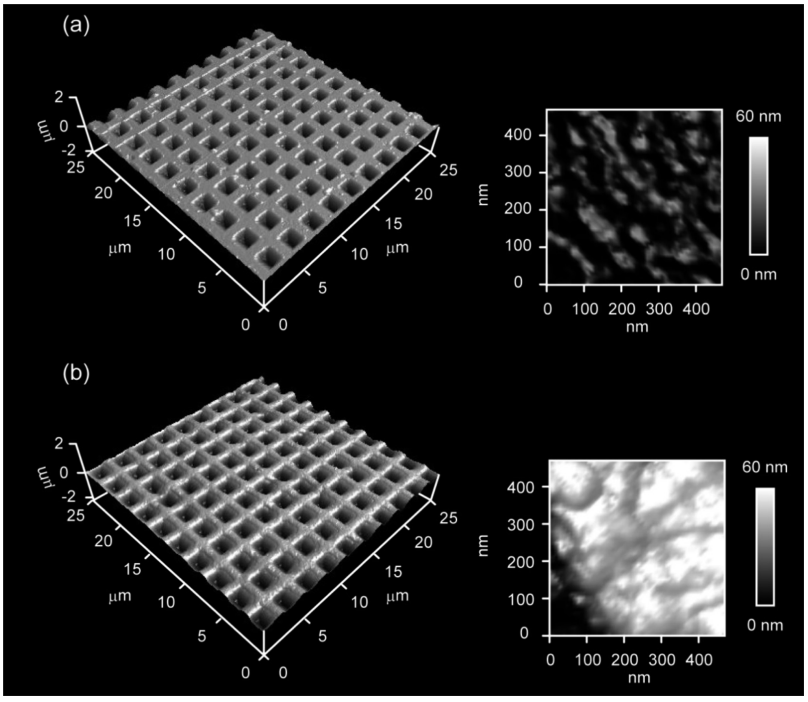

Figure 2. Three-dimensional AFM images of (a) unmodified and (b) poly(Man-*r*-TMS)-immobilized MMDs. The images on the right side show two-dimensional AFM images of the grid surfaces.

tion of the poly(AcMan-*r*-TMS) was associated with an approximately 1.5-fold increase in the atomic percentage of carbon on the MMD (Table S1, Supporting Information). The atomic percentage of carbon on the poly(Man-*r*-TMS)-immobilized MMD was slightly reduced, compared with that on the poly(AcMan-*r*-TMS)-immobilized MMD, confirming that carbon atoms had been released from the polymer as a consequence of the deacetylation process, as expected. The contact angle data also revealed that the deacetylated surface was more hydrophilic than the poly(AcMan-*r*-TMS)-immobilized surface (Figure S3, Supporting Information) and provided further evidence that the deacetylation process had actually occurred. We also confirmed that the soluble AcMan homopolymer had been completely deacetylated under the same conditions.[32] The amount of poly(Man-*r*-TMS) immobilized on the MMD was determined to be 470 μg per sheet.

Three-dimensional AFM images of the MMD are shown in Figure 2. The surface of the unmodified MMD was flat and smooth (R_q of the grid surface: 13 ± 3 nm) and was observed as a lattice-shaped structure with an open length of 1.8 μm and a grid interval of 2.6 μm. When the poly(Man-*r*-TMS) layer was formed on the MMD, the grids were rounded (R_q of the grid surface: 55 ± 4 nm). It was possible to confirm the presence of poly(Man-*r*-TMS) on the MMD by visual inspection. The AFM image of the poly(Man-*r*-TMS)-immobilized MMD showed that the holes were not blocked; i.e., the lattice-shaped structure was maintained after forming the poly(Man-*r*-TMS) layer. The calculated thickness of the polymer layer was ca. 50 nm (Figure S4, Supporting Information).

3.2. Spectral-Transmission Characteristics of the Poly(Man-*r*-TMS)-Immobilized MMD. The transmittance IR spectra of the unmodified, poly(AcMan-*r*-TMS)-immobilized, and poly(Man-*r*-TMS)-immobilized MMDs are shown in Figure 3. In the transmittance spectra of the MMD with a two-

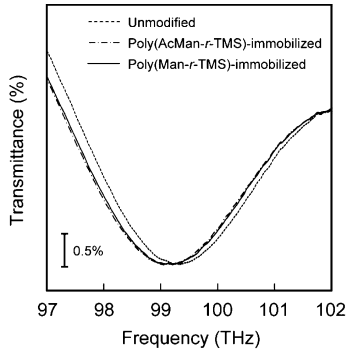

Figure 3. FT-IR spectra of unmodified, poly(AcMan-*r*-TMS)-immobilized, and poly(Man-*r*-TMS)-immobilized MMDs.

dimensionally periodic geometry, the dipped structure was observed around 100 THz. The localized electromagnetic field had an effect on the attachment of substance to the MMD. When poly(AcMan-*r*-TMS) was immobilized on the MMD, a red shift in the dipped frequency was observed, which was attributed to changes in the refractive index. Because the glycopolymer layer on the MMD was thin, the change in the transmittance was not observed ($-\Delta T < 0.5\%$). Following the deacetylation process, a slight blue shift was observed in the dipped frequency of the transmittance spectrum. The blue shift in the dipped frequency was attributed to a reduction in the attached amount, based on the assumption that the poly(AcMan-*r*-TMS) had been deacetylated. The dipped structures of the poly(AcMan-*r*-TMS)-immobilized and poly(Man-*r*-TMS)-immobilized MMDs also suggested that the lattice-shaped morphologies of the materials had been preserved. The poly(Man-*r*-TMS)-immobilized MMD could be operated in the middle-infrared region.

The thickness of the glycopolymer layer was determined to be 39 ± 2 nm by ellipsometry and was very close to that

calculated from the R_z difference between the unmodified and poly(Man-*r*-TMS)-immobilized MMDs. To estimate the $L_{1/e}$, the electromagnetic field distribution of the unmodified MMD was simulated using the TLM method (Figure S5, Supporting Information). The shape and dipped frequency in the simulated transmittance spectrum was close to those in the measured transmittance spectrum. The relative resonance energy of the electromagnetic field is shown in Figure 4. The energy of the

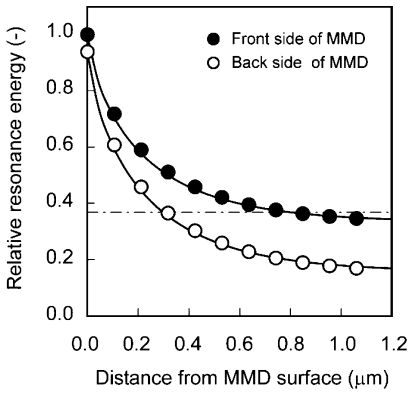

Figure 4. Simulated distribution of the electromagnetic field of the 100 THz-operated MMD along propagation direction of the incident wave. The dashed line represents the value of 0.368 $(1/e)$.

electromagnetic field decayed exponentially with moving from the localized surface. The $L_{1/e}$ values were 0.3−0.8 μm. The thickness of the poly(Man-*r*-TMS) layer and the length between the MMD surface and the protein analyte fell within the $L_{1/e}$. The simulations indicated that the shift behavior in the dipped frequency of the MMD depends on the material and the size of analyte (Figure S6, Supporting Information).

3.3. Detection of Protein Using the Poly(Man-*r*-TMS)-Immobilized MMD Sensor. The MMD sensor was measured to evaluate its ability to quantitatively detect the adsorption of protein on the poly(Man-*r*-TMS)-immobilized surface. The values of $-\Delta f$ for the Con A and BSA adsorptions are shown in Figure 5. BSA, which was used as a reference protein, was not adsorbed on the poly(Man-*r*-TMS)-immobilized MMD at any of the concentrations tested. In bioseparation research, poly(Man-*r*-TMS)-immobilized membranes have reduced the amount of BSA adsorption owing to the hydrophilic properties

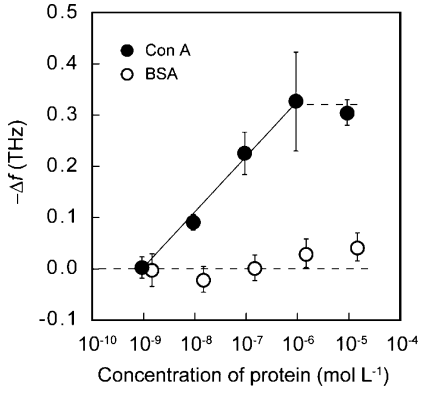

Figure 5. Changes in the dipped frequency in FT-IR spectra of the poly(Man-*r*-TMS)-immobilized MMD after adsorption of protein at different concentrations. The error bars represent the standard deviations, which were determined from four different samples.

of the saccharides moieties.[32] The prevention of nonspecific adsorption processes could also be advantageous for biosensing applications. The $-\Delta f$ value for Con A adsorption increased from 10^{-9} to 10^{-6} mol L^{-1}, where it reached saturation. The $-\Delta F$ values from the QCM measurements and the SPR responses for the Con A and BSA detections are shown in Figure 6. These results revealed that BSA was not adsorbed onto the poly(Man-*r*-TMS)-immobilized surface at any of the concentrations tested in the current study. The $-\Delta F$ values from QCM measurement and the SPR responses for Con A detection increased from 10^{-9} to 10^{-6} mol L^{-1}, which was comparable to the detection range observed for Con A using the poly(Man-*r*-TMS)-immobilized MMD. In the previous study, the detectability of the biotinylated MMD for streptavidin was close to those of biotinylated QCM.[6] These results indicated the relevance of the MMD sensor. Poly(Man-*r*-TMS) has been reported to exhibit strong and specific binding to Con A because of the glyco-cluster effect.[32] The AFM images showed that the holes on the surface of the MMD remained open following the adsorption of Con A (Figure S7, Supporting Information). The $-\Delta T$ values for Con A adsorption were less than 0.5%. Poly(Man-*r*-TMS)-immobilized MMDs, which had been stored for more than 1 year, retained their ability to selectively detect the adsorption of Con A (Figure S8, Supporting Information). This result represents a significant advantage to this synthetic polymer ligand compared with an antibody ligand. The amount of Con A adsorbed onto the MMD was determined by electrophoresis (Figure S9, Supporting Information). The $-\Delta f$ as a function of the amount of Con A adsorbed (q) is shown in Figure 7 The correlation between the $-\Delta f$ and q values was relatively linear. The detection limit of the MMD sensor for Con A was found to be 1 ng mm^{-2} (i.e., 10 fmol mm^{-2}). The saccharide-immobilized MMD, which could adsorb analytes in the vicinity of the surface, effectively behaved as a label-free biosensor exhibiting high levels of selectivity and sensitivity.

3.4. Detection of Bacterium Using a Poly(Man-*r*-TMS)-Immobilized MMD Sensor. The poly(Man-*r*-TMS)-immobilized MMD sensor was applied to quantitatively detect bacteria, which were used as model microsized analytes. The dipped frequency and transmittance in the spectra of the poly(Man-*r*-TMS)-immobilized MMD decreased as the concentration of ORN178 increased, whereas those did not decrease as the concentration of ORN208 increased (Figure S10, Supporting Information). The $-\Delta f$ value for the bacteria was high, compared with that for the protein detection. The $-\Delta f$ values for the ORN178 and ORN208 adhesions using the poly(Man-*r*-TMS)-immobilized MMD are shown in Figure 8a. ORN178 was detected at the *E. coli* concentration in excess of 10^6 cell mL^{-1} by the poly(Man-*r*-TMS)-immobilized MMD. The detection limit of the MMD sensor for *E. coli* was comparable to that of quartz crystal microbalance using a Man-self-assembled gold electrode.[45] The $-\Delta f$ value for the ORN208 strain, which did not contain the mannose receptor, remained unchanged at all of the concentrations tested in the current study. These results therefore indicated that the interaction between poly(Man-*r*-TMS) and the ORN178 strain of *E. coli* was specific. When ORN178 was adhered at 10^9 cell mL^{-1}, the holes of the MMD were closed by *E. coli* (Figure S11, Supporting Information), resulting in the disappearance of the dipped structure in the transmittance spectra. For microsized analytes such as *E. coli*, reductions in the transmittance of the dipped structure in the spectra of the poly(Man-*r*-TMS)-

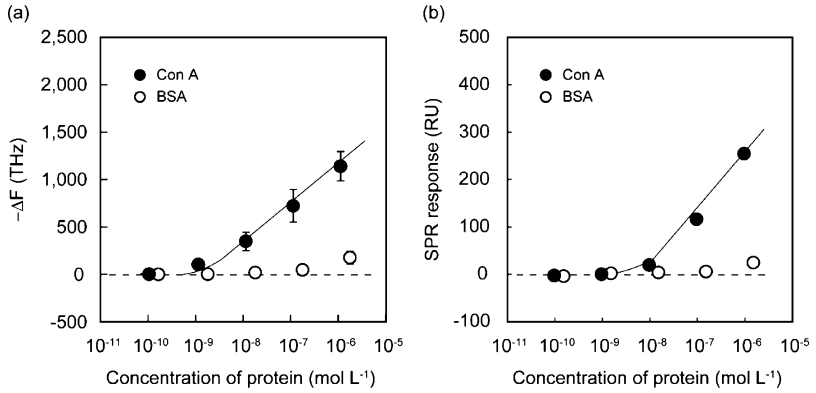

Figure 6. Detections of Con A and BSA on the poly(Man-*r*-TMS)-immobilized surface using (a) QCM and (b) SPR measurements. The error bars in the QCM represent the standard deviations, which were determined from three different samples.

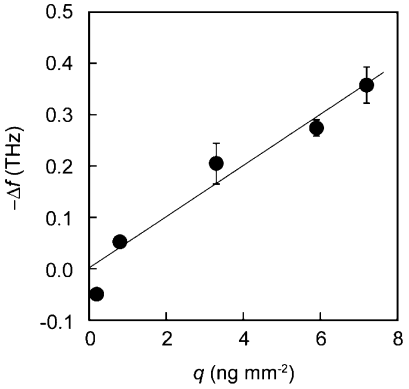

Figure 7. Changes in the dipped frequency of the FT-IR spectra of the MMD after adsorption of Con A versus the amount of Con A adsorbed on the poly(Man-*r*-TMS)-immobilized MMD. The solid line represents the straight-line approximation ($-\Delta f = 0.05 \times q$, $R^2 = 0.9473$). The error bars represent the standard deviations, which were determined from two different samples.

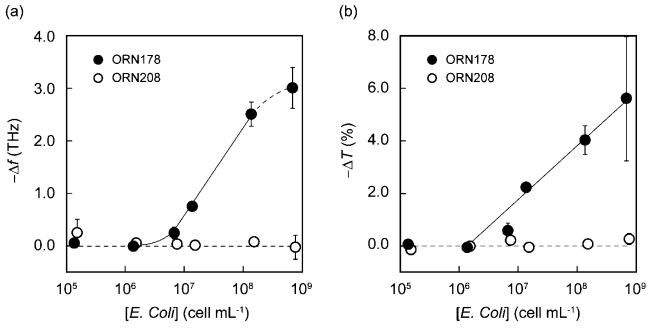

Figure 8. Changes in the (a) dipped frequency and (b) transmittance in FT-IR spectra of the poly(Man-*r*-TMS)-immobilized MMD after adhesion of *E. coli* ORN178 and ORN208 at different concentrations. The error bars represent the standard deviations, which were determined from two different samples.

immobilized MMD were noticeable, compared with nanosized analyst such as protein. The $-\Delta T$ values for the adhesion of ORN178 and ORN208 to the poly(Man-*r*-TMS)-immobilized MMD are also shown in Figure 8b. Similarly to the $-\Delta f$ values, the $-\Delta T$ values for ORN178 increased at *E. coli* concentrations greater than 10^6 cell mL^{-1}, whereas the $-\Delta T$ value for ORN208 remained unchanged for all of the concentrations tested in the current study. The poly(Man-*r*-TMS)-immobilized MMD sensor could therefore be used to specifically and extensively detect bacteria as well as proteins. We recently succeeded in the collection and detection of microparticles from air using the MMDs.[46] Given that analyte solutions could readily permeate though the large number of holes on the surface of an MMD, it is envisaged that the MMDs will find numerous applications as fluidic devices for the detection of bacteria.

4. CONCLUSIONS

A poly(Man-*r*-TMS)-immobilized MMD sensor has been evaluated for its ability to detect proteins and bacteria. The poly(Man-*r*-TMS) was immobilized on a nickel MMD using a silane coupling reaction. The poly(Man-*r*-TMS)-immobilized MMD sensor was used to achieve high levels of selectively and sensitively for the detection of a protein and a bacterium. Various pathogens, such as influenza viruses, human immunodeficiency viruses, *E. coli* O157 Shiga toxins, and cholera toxins, are recognized by saccharides on cell surfaces. It is, therefore, expected that glycopolymer-immobilized MMD sensors detect these pathogens. The MMD biosensor possesses several key advantages, including having convenient surface modification, potential for miniaturization, high throughput, and a wide detection range and being label free and a nondestructive test. We are currently working toward developing practical applications for MMDs as biosensors in the medical and health care fields.

■ ASSOCIATED CONTENT

Supporting Information

Manufacture of the MMD; transmittance IR spectra of the original MMDs; characteristics of the poly(Man-*r*-TMS)-immobilized MMD; XPS wide-scan spectra; atomic percentages of the unmodified, poly(AcMan-*r*-TMS)-immobilized, and poly(Man-*r*-TMS)-immobilized MMDs; contact angle images; two-dimensional AFM images; simulation for the electromagnetic field distribution on the MMD using the TLM method; simulation for the effect of the target material and size on the dipped frequency using the TLM method; three-dimensional AFM image; FT-IR spectra of poly(Man-*r*-TMS)-immobilized MMDs; determination of the Con A concentration using electrophoresis; detection of *E. coli* using the poly(Man-*r*-TMS)-immobilized MMD sensor. This material is available free of charge via the Internet at http://pubs.acs.org.

AUTHOR INFORMATION

Corresponding Author

*Tel: +81-92-802-2749. Fax: +81-92-802-2769. E-mail: miuray@chem-eng.kyushu-u.ac.jp.

Notes

The authors declare no competing financial interest.

ACKNOWLEDGMENTS

This work was supported by a Grant-in-Aid for Challenging Exploratory Research (24655157), a Grant-in-Aid for Young Scientists (A) (23685027), and a JSPS Research Fellowship for Young Scientists. We thank Prof. A. Takahara at Kyushu University for providing access to the ellipsometry equipment.

REFERENCES

(1) Miyamaru, F.; Hayashi, S.; Otani, C.; Kawase, K.; Ogawa, Y.; Yoshida, H.; Kato, E. Terahertz Surface-Wave Resonant Sensor with a Metal Hole Array. *Opt. Lett.* **2006**, *31*, 1118−1120.

(2) Yoshida, H.; Ogawa, Y.; Kawai, Y.; Hayashi, S.; Hayashi, A.; Otani, C.; Kato, E.; Miyamaru, F.; Kawase, K. Terahertz Sensing Method for Protein Detection Using a Thin Metallic Mesh. *Appl. Phys. Lett.* **2007**, *91*, 253901−253903.

(3) Ogawa, Y.; Hayashi, S.; Otani, C.; Kawase, K. Terahertz Sensing for Ensuring the Safety and Security. *PIERS Online* **2008**, *4*, 396−400.

(4) Yoshida, S.; Kato, E.; Suizu, K.; Nakagomi, Y.; Ogawa, Y.; Kawase, K. Terahertz Sensing of Thin Poly(ethylene Terephthalate) Film Thickness Using a Metallic Mesh. *Appl. Phys. Express* **2009**, *2*, 012301.

(5) Kondo, T.; Kamba, S.; Takigawa, K.; Suzuki, T.; Ogawa, Y.; Kondo, N. Highly Sensitive Metal Mesh Sensors. *Procedia Eng.* **2011**, *25*, 916−919.

(6) Seto, H.; Yamashita, C.; Kamba, S.; Kondo, T.; Hasegawa, M.; Matsuno, M.; Ogawa, Y.; Hoshino, Y.; Miura, Y. Biotinylation of Silicon and Nickel Surfaces and Detection of Streptavidin as Biosensor. *Langmuir* **2013**, *29*, 9457−9463.

(7) Yoshida, S.; Suizu, K.; Kato, E.; Nakagomi, Y.; Ogawa, Y.; Kawase, K. A High-Sensitivity Terahertz Sensing Method Using a Metallic Mesh with Unique Transmission Properties. *J. Mol. Spectrosc.* **2009**, *256*, 146−151.

(8) Suzuki, T.; Kondo, T.; Ogawa, Y.; Kamba, S.; Kondo, N. Detection of SiO_2 Thin Layer by Using a Metallic Mesh Sensor. *IEEE Sens. J.* **2013**, *13*, 4972−4976.

(9) Taylor, M. E.; Drickamer, K. In *Introduction to Glycobiology*, 2nd Ed.; Oxford University Press: Oxford, 2002.

(10) Lee, C. Y.; Lee, T. R. Carbohydrate-Protein Interactions: Basis of Glycobiology. *Acc. Chem. Res.* **1995**, *28*, 321−327.

(11) Choi, S.-K.; Mammen, M.; Whitesides, G. M. Generation and in Situ Evaluation of Libraries of Poly(acrylic acid) Presenting Sialosides as Side Chains as Polyvalent Inhibitors of Influenza-Mediated Hemagglutination. *J. Am. Chem. Soc.* **1997**, *119*, 4103−4111.

(12) Mammen, M.; Choi, S.-K.; Whitesides, G. M. Polyvalent Interactions in Biological Systems: Implications for Design and Use of Multivalent Ligands and Inhibitors. *Angew. Chem., Int. Ed.* **1998**, *37*, 2754−2794.

(13) Miura, Y. Design and Synthesis of Well-Defined Glycopolymers for the Control of Biological Functionalities. *Polym. J.* **2012**, *44*, 679−689.

(14) Jelinek, R.; Kolusheva, S. Carbohydrate Biosensors. *Chem. Rev.* **2004**, *104*, 5987−6016.

(15) Horlacher, T.; Seeberger, P. H. Carbohydrate Arrays as Tools for Research and Diagnostics. *Chem. Soc. Rev.* **2008**, *37*, 1414−1422.

(16) Vikesland, P. J.; Wigginton, K. R. Nanomaterial Enabled Biosensors for Pathogen Monitoring-A Review. *Environ. Sci. Technol.* **2010**, *44*, 3656−3669.

(17) Cheng, C.-I.; Chang, Y.-P.; Chu, Y.-H. Biomolecular Interactions and Tools for Their Recognition: Focus on the Quartz Crystal Microbalance and its Diverse Surface Chemistries and Applications. *Chem. Soc. Rev.* **2012**, *41*, 1947−1971.

(18) Zeng, X.; Andrade, C. A. S.; Oliveira, M. D. L.; Sun, X.-L. Carbohydrate-Protein Interactions and their Biosensing Applications. *Anal. Bioanal. Chem.* **2012**, *402*, 3161−3176.

(19) Ali, M.; Nasir, S.; Ramirez, P.; Cervera, J.; Mafe, S.; Ensinger, W. Carbohydrate-Mediated Biomolecular Recognition and Gating of Synthetic Ion Channels. *J. Phys. Chem. C* **2013**, *117*, 18234−18242.

(20) Kotsuchibashi, Y.; Zhang, Y.; Ahmed, M.; Ebara, M.; Aoyagi, T.; Narain, R. Fabrication of FITC-Doped Silica Nanoparticles and Study of their Cellular Uptake in the Presence of Lectins. *J. Biomed. Mater. Res., Part A* **2013**, *101A*, 2090−2096.

(21) Nagatsuka, T.; Uzawa, H.; Sato, K.; Kondo, S.; Izumi, M.; Yokoyama, K.; Ohsawa, I.; Seto, Y.; Neri, P.; Mori, H.; Nishida, Y.; Saito, M.; Tamiya, E. Localized Surface Plasmon Resonance Detection of Biological Toxins Using Cell Surface Oligosaccharides on Glyco Chips. *ACS Appl. Mater. Interfaces* **2013**, *5*, 4173−4180.

(22) Reichardt, N. C.; Martín-Lomas, M.; Penadés, S. Glyconanotechnology. *Chem. Soc. Rev.* **2013**, *42*, 4358−4376.

(23) Zhang, H.; Zhang, L.; Liang, R. P.; Huang, J.; Qiu, J. D. Simultaneous Determination of Concanavalin A and Peanut Agglutinin by Dual-Color Quantum Dots. *Anal. Chem.* **2013**, *85*, 10969−10976.

(24) Chevolot, Y.; Laurenceau, E.; Phaner-Goutorbe, M.; Monnier, M.; Souteyrand, E.; Meyer, A.; Gehin, T.; Vasseur, J. J.; Morvan, F. DNA Directed Immobilization Glycocluster Array: Applications and Perspectives. *Curr. Opin. Chem. Biol.* **2014**, *18*, 46−54.

(25) Gerland, B.; Goudot, A.; Ligeour, C.; Pourceau, G.; Meyer, A.; Vidal, S.; Gehin, T.; Vidal, O.; Souteyrand, E.; Vasseur, J. J.; Chevolot, Y.; Morvan, F. Structure Binding Relationship of Galactosylated Glycoclusters toward *Pseudomonas aeruginosa* Lectin LecA Using a DNA-Based Carbohydrate Microarray. *Bioconjugate Chem.* **2014**, *25*, 379−392.

(26) Pawlak, M.; Mistlberger, G.; Bakker, E.; Concanavalin, A. Electrochemical Sensor Based on the Surface Blocking Principle at an Ion-Selective Polymeric Membrane. *Microchim. Acta* **2014**, DOI: 10.1007/s00604-014-1309-3.

(27) Babiuch, K.; Stenzel, M. H. In *Encyclopedia of Polymer Science and Engineering*; Wiley: New York, 2014; DOI: 10.1002/0471440264.

(28) Miura, Y.; Seto, H.; Fukuda, T. In *An Integrated View of the Molecular Recognition and Toxinology - From Analytical Procedures to Biomedical Applications*; Rádis-Baptista, G., Ed.; InTech: Rijeka, 2013; pp 455−470.

(29) Ishii, J.; Toyoshima, M.; Chikae, M.; Takayura, Y.; Miura, Y. Preparation of Glycopolymer-Modified Gold Nanoparticles and a New Approach for a Lateral Flow Assay. *Bull. Chem. Soc. Jpn.* **2011**, *84*, 466−470.

(30) Takara, M.; Toyoshima, M.; Seto, H.; Hoshino, Y.; Miura, Y. Polymer-Modified Gold Nanoparticles via RAFT Polymerization: A Detailed Study for a Biosensing Application. *Polym. Chem.* **2014**, *5*, 931−939.

(31) Terada, Y.; Hashimoto, W.; Endo, T.; Seto, H.; Murakami, T.; Hisamoto, H.; Hoshino, Y.; Miura, Y. Signal Amplified Two-Dimensional Photonic Crystal Biosensor Immobilized with Glyco-Nanoparticles. *J. Mater. Chem. B* **2014**, *2*, 3324−3332.

(32) Seto, H.; Ogata, Y.; Murakami, T.; Hoshino, Y.; Miura, Y. Selective Protein Separation Using Siliceous Materials with a Trimethoxysilane-Containing Glycopolymer. *ACS Appl. Mater. Interfaces* **2012**, *4*, 411−417.

(33) Ogata, Y.; Seto, H.; Murakami, T.; Hoshino, Y.; Miura, Y. Affinity Separation of Lectins Using Porous Membranes Immobilized with Glycopolymer Brushes Containing Mannose or *N*-Acetyl-D-Glucosamine. *Membranes* **2013**, *3*, 169−181.

(34) Seto, H.; Takara, M.; Yamashita, C.; Murakami, T.; Hasegawa, T.; Hoshino, Y.; Miura, Y. Surface Modification of Siliceous Materials Using Maleimidation and Various Functional Polymers Synthesized by Reversible Addition-Fragmentation Chain Transfer Polymerization. *ACS Appl. Mater. Interfaces* **2012**, *4*, 5125−5133.

(35) Kim, E. J.; Shin, H.-Y.; Park, S.; Sung, D.; Jon, S.; Sampathkumar, S.-G.; Choi, S. Y.; Kim, K. Electrochemically Active, Anti-Biofouling Polymer Adlayers on Indium-Tin-Oxide Electrodes. *Chem. Commun.* **2008**, 3543−3545.
(36) Shah, S. S.; Howland, M. C.; Chen, L.-J.; Silangcruz, J.; Verkhoturov, S. V.; Schweikert, E. A.; Parikh, A. N.; Revzin, A. Micropatterning of Proteins and Mammalian Cells on Indium Tin Oxide. *ACS Appl. Mater. Interfaces* **2009**, *1*, 2592−2601.
(37) Choi, H. W.; Sakata, Y.; Kurihara, Y.; Ooya, T.; Takeuchi, T. Label-Free Detection of C-Reactive Protein Using Reflectometric Interference Spectroscopy-Based Sensing System. *Anal. Chim. Acta* **2012**, *728*, 64−68.
(38) Endo, T.; Sato, M.; Kajita, H.; Okuda, N.; Tanaka, S.; Hisamoto, H. Printed Two-Dimensional Photonic Crystals for Single-Step Label-Free Biosensing of Insulin under Wet Conditions. *Lab Chip* **2012**, *12*, 1995−1999.
(39) Fu, H.; Dencic, I.; Tibhe, J.; Sanchez Pedraza, C. A.; Wang, Q.; Noel, T.; Meuldijk, J.; de Croon, M.; Hessel, V.; Weizenmann, N.; Oeser, T.; Kinkeade, T.; Hyatt, D.; Van Roy, S.; Dejonghe, W.; Diels, L. Threonine Aldolase Immobilization on Different Supports for Engineering of Productive, Cost-Efficient Enzymatic Microreactors. *Chem. Eng. J.* **2012**, *207−208*, 564−576.
(40) Tarannum, N.; Singh, M. Water-Compatible Surface Imprinting of 'Baclofen' on Silica Surface for Selective Recognition and Detection in Aqueous Solution. *Anal. Methods* **2012**, *4*, 3019−3026.
(41) Bañuls, M. J.; Puchades, R.; Maquieira, Á. Chemical Surface Modifications for the Development of Silicon-Based Label-Free Integrated Optical (IO) Biosensors: A Review. *Anal. Chim. Acta* **2013**, *777*, 1−16.
(42) He, Q.; Ma, C.; Hu, X.; Chen, H. Method for Fabrication of Paper-Based Microfluidic Devices by Alkylsilane Self-Assembling and UV/O_3-Patterning. *Anal. Chem.* **2013**, *85*, 1327−1331.
(43) Harris, S. L.; Spears, P. A.; Havell, E. A.; Hamrick, T. S.; Horton, J. R.; Orndorff, P. E. Characterization of *Escherichia coli* Type 1 Pilus Mutants with Altered Binding Specificities. *J. Bacteriol.* **2011**, *183*, 4099−4102.
(44) Grosvenor, A. P.; Biesinger, M. C.; Smart, R. S.; McIntyre, N. S. New Interpretations of XPS Spectra of Nickel Metal and Oxides. *Surf. Sci.* **2006**, *600*, 1771−1779.
(45) Shen, Z.; Huang, M.; Xiao, C.; Zhang, Y.; Zeng, X.; Wang, P. G. Nonlabeled Quartz Crystal Microbalance Biosensor for Bacterial Detection Using Carbohydrate and Lectin Recognitions. *Anal. Chem.* **2007**, *79*, 2312−2319.
(46) Seto, H.; Kamba, S.; Kondo, T.; Ogawa, Y.; Hoshino, Y.; Miura, Y. Novel Detection Technique for Particulate Matter in Air Using Metal Mesh Device Sensors. *Chem. Lett.* **2014**, *43*, 408−410.